

# 2D Internal Gravity Wave Turbulence

V. Labarre<sup>1,3</sup>† and M. Shavit<sup>2</sup>‡

<sup>1</sup>Université Côte d'Azur, Observatoire de la Côte d'Azur, CNRS, Laboratoire Lagrange, Boulevard de l'Observatoire CS 34229–F 06304 Nice Cedex 4, France

<sup>2</sup>Courant Institute of Mathematical Sciences, New York University, NY 10012, USA

<sup>3</sup>LadHyX, CNRS, École polytechnique, Institut polytechnique de Paris, 91120, Palaiseau, France

(Received xx; revised xx; accepted xx)

Using weak wave turbulence theory analysis, we distinguish three main regimes for 2D stratified fluids in the dimensionless parameter space defined by the Froude number and the Reynolds number: discrete wave turbulence, weak wave turbulence, and strong nonlinear interaction. These regimes are investigated using direct numerical simulations (DNS) of the 2D Boussinesq equations with shear modes removed. In the weak wave turbulence regime, excluding slow frequencies, we observe a spectrum that aligns with recent predictions from kinetic theory. This finding represents the first DNS-based confirmation of wave turbulence theory for internal gravity waves. At strong stratification, in both the weak and strong interaction regimes, we observe the formation of layers accompanied by spectral peaks at low discrete frequencies. We explain this layering through an inverse kinetic energy cascade and the discreteness of wave-wave interactions at large scales. This analysis allows us to predict the layer thickness and typical flow velocity in terms of the control parameters.

**Key words:** Stratified Turbulence, Wave-turbulence interactions, Wave breaking.

## 1. Introduction

Internal gravity waves propagating within stably stratified fluids are ubiquitous in geophysical and astrophysical systems. Through the transport of mass, momentum, and energy, they play a crucial role in shaping oceanic and atmospheric circulations (Andrews *et al.* 1987; Bühler 2014; Vallis 2017; Whalen *et al.* 2020) and influence the internal dynamics of stars (Rogers *et al.* 2013). Recent studies have shown the significant impact of diapycnal mixing, driven by internal gravity waves, on various climate phenomena. However, accurately resolving the short vertical scales involved -particularly in climate simulations- remains challenging. It highlights the importance of theoretical modeling and further study of internal gravity waves (MacKinnon *et al.* 2017).

For strongly dispersive waves, as long as amplitudes are small, the weak wave turbulence theory allows writing a closed kinetic equation for the slow evolution of the averaged spectral energy density (Hasselmann 1966; Zakharov *et al.* 1992; Nazarenko 2011; Newell & Rumpf 2011; Galtier 2022). The first kinetic equation for 3D internal waves, with rotation, was written by Olbers (1976). Since then, it has been re-derived using various formalisms and assumptions, see e.g. (Pelinovsky & Raevsky 1977; Müller *et al.* 1986; Caillol & Zeitlin 2000; Lvov & Tabak 2001, 2004; Lvov *et al.* 2012; Scott & Cambon 2024; Labarre *et al.* 2024b). At zero rotation, by applying the hydrostatic approximation -which assumes long horizontal scales compared to

† Email address for correspondence: vincent.labarre@polytechnique.edu

‡ Email address for correspondence: ms14479@nyu.edu

vertical scales- several authors found a formal steady spectrum (Pelinovsky & Raevsky 1977; Caillol & Zeitlin 2000; Lvov & Tabak 2001). But this spectrum is not a physically realizable solution, as noted by Caillol & Zeitlin (2000). Later, Lvov *et al.* (2010); Dematteis & Lvov (2021) showed that there is only one bi-homogeneous steady spectrum that yields a converging collision integral. Yet, this 3D theoretical prediction has never been observed directly. Still in the hydrostatic approximation, Lanchon & Cortet (2023) have found a solution to a diffusion approximation of the kinetic equation retaining only induced diffusion triads interactions (McComas & Bretherton 1977). In 2D, using a more general approach, Shavit *et al.* (2024) found a steady solution of the full kinetic equation without the hydrostatic approximation. Namely, the steady energy spectrum is

$$e(\mathbf{k}) \propto k^{-3} |\omega_{\mathbf{k}}|^{-2} \quad (1.1)$$

where  $\mathbf{k} = (k_x, k_z)$  is the wave vector,  $k = \sqrt{k_x^2 + k_z^2}$  its modulus,  $\omega_{\mathbf{k}} = Nk_x/k$  the internal gravity wave frequency, and  $N$  is the buoyancy frequency. Changing coordinates, this is the oceanic Garrett-Munk (GM) spectrum (Garrett & Munk 1979) in the limit of zero rotation and short vertical scales compared to the ocean depth

$$k^{-3} (\omega_{\mathbf{k}}/N)^{-2} dk_x dk_z = k_z^{-2} (\omega_{\mathbf{k}}/N)^{-2} dk_z d\omega_{\mathbf{k}} \propto e_{GM}. \quad (1.2)$$

Despite deviations from the empirical GM spectrum of measured spectra of oceanic internal gravity waves, it is still considered to be a useful description of oceanic internal gravity waves (Polzin *et al.* 2014; Dematteis *et al.* 2024).

Similar to other anisotropic dispersive waves in fluids, such as Rossby and inertial waves, internal gravity waves interact with slow modes, specifically domain vortical and shear modes (Smith & Waleffe 2002; Laval *et al.* 2003; Brethouwer *et al.* 2007; Waite 2011; Rempel *et al.* 2014; Howland *et al.* 2020; Rodda *et al.* 2022). These slow modes present a significant challenge for the current weak wave turbulence description, which does not account for their evolution or interaction with dispersive waves. Their prominence in the energy spectrum complicates the observation of weak wave turbulence in internal gravity waves, both in direct numerical simulations (Rempel *et al.* 2014) and experiments (Lanchon *et al.* 2023). In particular, a well-observed feature of stratified turbulence is layering (see Caulfield (2021) and references therein), corresponding to an accumulation of energy in horizontal motions (shear and vortical modes) with the formation of well-mixed layers separated by sharp interfaces. If turbulence and stratification are strong enough, the layers' thickness is "chosen" by the flow such that  $L_z = U/N$ , where  $U$  is the typical velocity of the flow (Billant & Chomaz 2001; Brethouwer *et al.* 2007). This phenomenon looks like a self-organised criticality, where the flow organizes itself such that the Richardson number is close to a critical value (Caulfield 2021), not too far from the linear stability threshold (Miles 1961; Howard 1961).

One advances several mechanisms to explain the layering in strongly stratified turbulence. Phillips (1972) proposed a simple model for the evolution of the average vertical density profile, illustrating how layers could develop from small perturbations to an initially linear density profile. He showed that if the magnitude of the buoyancy flux is a decreasing function of the local gradient Richardson number, small disturbances to the initial stratification profile can grow in time. Balmforth *et al.* (1998) used a reduced model based on two coupled partial differential equations for the average turbulent kinetic energy and the mean buoyancy, and a mixing length model. Taylor & Zhou (2017) have reformulated the conditions for amplifying small perturbations to a uniform stratification first proposed by Phillips and introduced a criterion for the development of layering in terms of the spatial distribution of appropriate eddy diffusivity. Petropoulos *et al.* (2023) used reduced-order models for the evolution of velocity and density gradients and analysed layering in stratified and sheared turbulent flows. They determined the ranges of bulk Richardson numbers and turbulent Prandtl numbers for layering. Billant & Chomaz (2000*a,b*) showed that

vortical modes are prone to zigzag instability, which leads to layering on the scale of  $U/N$ . Interestingly, one observes the layering in 2D (Smith 2001), as well as 3D without vortical modes (Rommel *et al.* 2014), or without vortical modes and shear modes (Calpe Linares 2020; Labarre *et al.* 2024a). Also, Fitzgerald & Farrell (2018a) showed that stochastic structural stability theory (Farrell & Ioannou 2003) and quasi-linear turbulence closures reproduce layering in the 2D case. Therefore, it is worth searching for a weak wave turbulence explanation of the layering process.

In the present study, we employ 2D DNS of the Boussinesq equations, removing slow (shear) modes. Our prime goal is to identify the parameter regime for observing weak wave turbulence, report fundamental features of the fields in the weak wave turbulence regime - mainly the energy spectrum and the associated energy flux and compare these to the theoretical predictions. We remove shear modes to reach the steady state faster and have a cleaner comparison to weak wave turbulence predictions. The reason to consider 2D flows is twofold – from the practical point of view it is much cheaper and faster compared to 3D DNS. From the theoretical point of view, the kinetic equation for 2D (Shavit *et al.* 2023), takes a simpler form compared to 3D due to the existence of an additional invariant and has a theoretical prediction of the spectrum outside the hydrostatic limit. Despite being an important simplification when compared to real 3D flows, 2D stratified flows capture important aspects of stratified flows and often serve as an important step towards understanding the 3D problem (Smith 2001; Boffetta *et al.* 2011; Fitzgerald & Farrell 2018b; Calpe Linares 2020). Also, a 2D description of internal gravity waves is practically relevant both for experiments, e.g. in long water tanks, and in the ocean in the case of internal tides radiated away from isolated 1D topography structures such as the Hawaiian ridge (Smith & Young 2003). In the weak wave turbulence regime, excluding low frequencies, we observe a good agreement with the recent theoretical weak wave turbulence prediction (Shavit *et al.* 2024). As layering kicks in with spectral peaks observed at slow frequencies, our work emphasizes the limitation of the kinetic approach. Yet, our work advances beyond the weak interaction regime, and gives a simple explanation for layering (with scalings for  $U$  and  $L_z$  based on control parameters) even beyond the weakly non-linear regimes.

The remaining parts of the manuscript are as follows. In section 2, we introduce the dynamical equations and our notations. In section 3, we use wave turbulence theory to identify the three regimes: discrete wave turbulence, weak wave turbulence, and strong nonlinear interaction. This emphasizes that to observe the weak wave turbulence regime in a stratified fluid a directed study must be done, which is crucial for experiments and future numerical investigations. We describe our numerical simulations in section 4, and we analyse them in section 5. We present vorticity fields for different stratification and viscosity in subsection 5.1. Then, we show the 1D energy spectra for the regimes in subsection 5.2. In subsection 5.3, we analyse in more detail the 2D energy spectra and energy fluxes of a strongly nonlinear simulation. We provide a weak wave turbulence explanation to explain the layering process in subsection 5.4. In subsection 5.5, we analyse the 2D energy spectra and energy fluxes of a weakly nonlinear simulation and compare it to the theoretical predictions of Shavit *et al.* (2024). We describe the Doppler shift observed in some of our simulations in subsection 5.6. Section 6 contains discussions and conclusions.

## 2. Governing equations

### 2.1. Dynamical equations

Stratified flows can be described most simply using the Boussinesq equations, derived from the Euler equations by assuming a linear density profile in the vertical direction. For two-dimensional

flows restricted to the vertical  $xz$  plane, the Boussinesq equations are

$$\nabla \cdot \mathbf{u} = 0, \quad (2.1)$$

$$\partial_t \mathbf{u} + \mathbf{u} \cdot \nabla \mathbf{u} = -\nabla p + b \mathbf{e}_z \quad (2.2)$$

$$\partial_t b + \mathbf{u} \cdot \nabla b = -N^2 u_z, \quad (2.3)$$

where  $x$  and  $z$  are respectively the horizontal and vertical coordinates,  $\mathbf{u} = (u_x, u_z)$  is the velocity field,  $p$  the kinematic pressure,  $b$  the buoyancy, and  $N$  is the constant buoyancy (or Brünt-Väisälä) frequency. It is easy to check that (2.1-2.3) have two exact quadratic invariants: the total energy  $E = \frac{1}{2} \int dx dz \left( \mathbf{u} \cdot \mathbf{u} + \frac{b^2}{N^2} \right)$  and the correlation between vorticity,  $\nabla^\perp \times \mathbf{u}$ , and the buoyancy, called pseudomomentum  $P = - \int dx dz (\nabla^\perp \times \mathbf{u}) b$ . We consider a periodic domain  $\mathbf{x} = (x, z) \in [0, L]^2$  and expand the fields in terms of linear wave modes with wave vector  $\mathbf{k} \in (2\pi\mathbb{Z}/L)^2$ . In polar coordinates,  $\mathbf{k} = k(\cos \theta, \sin \theta)$ , the dispersion relation is

$$\omega_{\mathbf{k}} = N \cos \theta. \quad (2.4)$$

Since the nonlinearity is quadratic, a resonant interaction of internal gravity waves is a triad  $(\mathbf{k}, \mathbf{p}, \mathbf{q})$  satisfying

$$\omega_{\mathbf{k}} \pm \omega_{\mathbf{p}} \pm \omega_{\mathbf{q}} = 0. \quad (2.5)$$

We set  $L = 2\pi$ , so the  $x, z$  components of the wave vectors are integers.

## 2.2. Forcing, dissipation and energy transfers

We add forcing and dissipation to the dynamical equations to study the statistics of stationary turbulent states. Specifically, we force the system (2.1-2.3) at small wave vectors and add significant dissipation at large wave vectors. Rewriting the dynamical equations in terms of the stream function  $\psi$ ,  $(u_x, u_z) = (-\partial_z \psi, \partial_x \psi)$ , with forcing and dissipation yields

$$\partial_t \Delta \psi + \{\psi, \Delta \psi\} = \partial_x b + \Delta f_\psi + (-1)^{n-1} \nu_n \Delta^n (\Delta \psi), \quad (2.6)$$

$$\partial_t b + \{\psi, b\} = -N^2 \partial_x \psi + f_b + (-1)^{n-1} \kappa_n \Delta^n b. \quad (2.7)$$

Here  $-\Delta \psi$  is the vorticity,  $\{g, f\} = \partial_x g \partial_z f - \partial_z g \partial_x f$ .  $f_\psi$  and  $f_b$  are respectively the stream function and buoyancy forcing.  $\nu_n$  is the hyperviscosity and  $\kappa_n$  the hyperdiffusivity. In this study, we set  $\kappa_n = \nu_n$ . One recovers the standard Boussinesq equations for  $n = 1$ . Using hyperviscosity and hyperdiffusion is a standard method to enlarge the inertial range at a given resolution (Brethouwer *et al.* 2007).

In Fourier space, equations (2.6-2.7) read

$$\partial_t \hat{\psi}_{\mathbf{k}} - \frac{1}{k^2} \overline{\{\psi, \Delta \psi\}}_{\mathbf{k}} = i \frac{k_x}{k^2} \hat{b}_{\mathbf{k}} + \hat{f}_{\psi, \mathbf{k}} + (-1)^{n-1} \nu_n (-k^2)^n \hat{\psi}_{\mathbf{k}} \quad (2.8)$$

$$\partial_t \hat{b}_{\mathbf{k}} + \overline{\{\psi, b\}}_{\mathbf{k}} = i k_x N^2 \hat{\psi}_{\mathbf{k}} + \hat{f}_{b, \mathbf{k}} + (-1)^{n-1} \kappa_n (-k^2)^n \hat{b}_{\mathbf{k}} \quad (2.9)$$

where  $(\cdot)_{\mathbf{k}}$  denotes the Fourier transform. It follows that the equations for the kinetic energy spectrum  $e_{\text{kin}}(\mathbf{k}) = \langle |\hat{\mathbf{u}}_{\mathbf{k}}|^2 \rangle / 2 = k^2 \langle |\hat{\psi}_{\mathbf{k}}|^2 \rangle / 2$  and the potential energy spectrum  $e_{\text{pot}}(\mathbf{k}) = \langle |\hat{b}_{\mathbf{k}}|^2 \rangle / (2N^2)$  are

$$\partial_t e_{\text{kin}}(\mathbf{k}) = \mathcal{T}_{\text{kin}}(\mathbf{k}) - \Im \langle k_x \hat{b}_{\mathbf{k}} \hat{\psi}_{\mathbf{k}}^* \rangle + \Re \langle k^2 \hat{f}_{\psi, \mathbf{k}} \hat{\psi}_{\mathbf{k}}^* \rangle + (-1)^{n-1} \nu_n (-k^2)^n e_{\text{kin}}(\mathbf{k}), \quad (2.10)$$

$$\partial_t e_{\text{pot}}(\mathbf{k}) = \mathcal{T}_{\text{pot}}(\mathbf{k}) + \Im \langle k_x \hat{b}_{\mathbf{k}} \hat{\psi}_{\mathbf{k}}^* \rangle + \frac{1}{N^2} \Re \langle \hat{f}_{b, \mathbf{k}} \hat{b}_{\mathbf{k}}^* \rangle + (-1)^{n-1} \kappa_n (-k^2)^n e_{\text{pot}}(\mathbf{k}), \quad (2.11)$$

where  $\langle \cdot \rangle$  is an ensemble average (here a time average in statistically steady state),  $(\cdot)^*$  is the

complex conjugate,  $\Re(\cdot)$  is the real part,  $\Im(\cdot)$  is the imaginary part, and the kinetic and potential energy transfers are defined by

$$\mathcal{T}_{\text{kin}}(\mathbf{k}) = \Re \left\langle \hat{\psi}_{\mathbf{k}}^* \widehat{\{\psi, \Delta\psi\}}_{\mathbf{k}} \right\rangle \quad \text{and} \quad \mathcal{T}_{\text{pot}}(\mathbf{k}) = -\Re \left\langle \hat{b}_{\mathbf{k}}^* \widehat{\{\psi, b\}}_{\mathbf{k}} \right\rangle \quad (2.12)$$

respectively. Physically,  $\mathcal{T}_{\text{kin}}$  and  $\mathcal{T}_{\text{pot}}$  represent the kinetic and potential energy transfers to mode  $\mathbf{k}$  through nonlinear interactions per unit time. We denote the total energy spectrum  $e(\mathbf{k}) = e_{\text{kin}}(\mathbf{k}) + e_{\text{pot}}(\mathbf{k})$ , the total energy transfer  $\mathcal{T}(\mathbf{k}) = \mathcal{T}_{\text{kin}}(\mathbf{k}) + \mathcal{T}_{\text{pot}}(\mathbf{k})$ . We note the 1D kinetic energy transfers as

$$\mathcal{T}_{\text{kin}}(k) = \sum_{\mathbf{k}', |\mathbf{k}'| \leq k} \mathcal{T}_{\text{kin}}(\mathbf{k}'), \quad (2.13)$$

$$\mathcal{T}_{\text{kin}}(\omega_k) = \sum_{\mathbf{k}', |\omega_{\mathbf{k}'}| \leq \omega_k} \mathcal{T}_{\text{kin}}(\mathbf{k}'). \quad (2.14)$$

They represent respectively the kinetic energy transfer to modes with wave vector modulus less than  $k$  and the kinetic energy transfer to modes with wave frequency less than  $\omega_k$ . We use similar definitions for the 1D potential and total energy transfers.

We force the flow with two independent white noise terms for the stream function and the buoyancy for modes such that the forcing amplitudes are non-zero on a bounded ring  $|\mathbf{k}| \in [k_{f,\text{min}}, k_{f,\text{max}}]$  and  $k_x, k_y \neq 0$ . Without considering other terms but forcing, the dynamical equation for the stream function of forced modes reads

$$d\hat{\psi}_{\mathbf{k}} = \hat{f}_{\psi, \mathbf{k}} dt = \sqrt{\varepsilon} dt \frac{X_{\mathbf{k}} + X_{-\mathbf{k}}^*}{\sqrt{\sum_{\mathbf{k}} |X_{\mathbf{k}} + X_{-\mathbf{k}}^*|^2} k^2} \quad (2.15)$$

where  $X_{\mathbf{k}}$  are complex numbers whose real and imaginary parts are normal random variables. It ensures a real forcing in physical space with a constant average kinetic energy injection rate  $\sum_{\mathbf{k}} |\hat{f}_{\psi, \mathbf{k}} dt k|^2 / (2dt) = \varepsilon/2$ . The equivalent of equation (2.15) for the buoyancy is  $d\hat{b}_{\mathbf{k}} = \hat{f}_{b, \mathbf{k}} dt$  where  $\hat{f}_{b, \mathbf{k}}$  is obtained in the same way than  $\hat{f}_{\psi, \mathbf{k}}$ , up to a prefactor  $-Nk$ , and using an independent stochastic process. Doing so, the average potential energy injection is equal to  $\sum_{\mathbf{k}} \left| \frac{\hat{f}_{b, \mathbf{k}}}{N} dt \right|^2 / (2dt) = \varepsilon/2$ . The independence of  $f_{\psi}$  and  $f_b$  ensures that the pseudomomentum is zero on average,  $\langle P \rangle = 0$ . The parameters that quantify the forcing are therefore the average energy injection rate  $\varepsilon$ , and the wave vector modulus at the middle of the forcing ring  $k_f = (k_{f,\text{max}} + k_{f,\text{min}})/2$ .

### 3. Parametric regimes

The standard dimensionless parameters for a stratified fluid are the Froude number, which quantifies stratification strength, and the (hyper-viscous) Reynolds number, representing the balance between dissipation and non-linear interaction:

$$Fr \equiv \frac{U}{NL} \quad \text{and} \quad Re_n \equiv \frac{UL^{2n-1}}{\nu_n}, \quad (3.1)$$

where  $U$  is a typical velocity. We use  $U = (\varepsilon/k_f)^{1/3}$ , which differs from root mean square velocity used in many other studies (Billant & Chomaz 2001; Brethouwer *et al.* 2007). The Froude and Reynolds numbers determine fundamental flow length scales: the buoyancy and viscous scales.

These are associated with absolute wave vectors:

$$k_b \equiv \frac{N}{U} = \frac{Fr^{-1}}{L} \quad \text{and} \quad k_d \equiv \left( \frac{U}{v_n} \right)^{1/(2n-1)} = \frac{Re_n^{1/(2n-1)}}{L}. \quad (3.2)$$

For scales larger than  $2\pi/k_b$ , linear terms dominate over nonlinear ones in the dynamical equations (2.1-2.3), while at scales smaller than  $2\pi/k_d$ , dissipative terms dominate over nonlinear terms. The third central wave vector corresponds to the box size  $2\pi/L$ . We now identify three regimes: discrete wave turbulence, weak wave turbulence, and strong turbulence. To observe weak wave turbulence,

(i) Wave amplitudes must be small to ensure weak nonlinear interactions;

(ii) The number of pseudo-resonances -meaning resonances nearly satisfying (2.5)- needs to be large to ensure pseudo-continuous energy exchanges between waves (Bourouiba 2008; L'vov & Nazarenko 2010; Buckmaster *et al.* 2021).

Condition (i) is achieved if dissipation occurs at scales larger than the buoyancy scale, implying

$$k_d \lesssim k_b \Rightarrow Re_n \lesssim Fr^{-2n+1}. \quad (3.3)$$

Therefore, for weak wave turbulence to occur, the Reynolds number cannot be arbitrarily large, as shown in prior studies on internal wave turbulence (Le Reun *et al.* 2017, 2018; Brunet *et al.* 2020). When condition (3.3) is not met, wave breaking is likely, leading to strongly non-linear stratified turbulence. To ensure condition (ii), the frequency of the nonlinear interaction  $\omega_{nl}$  must exceed the wave frequency gap in discrete Fourier space  $|\nabla_{\mathbf{k}} \omega_{\mathbf{k}} \cdot d\mathbf{k}|$  with  $d\mathbf{k}$ , being the wave vector gap between adjacent modes (L'vov & Nazarenko 2010). Using dimensional analysis, we estimate  $\omega_{nl} = (\varepsilon k^2)^{1/3}$  and take  $d\mathbf{k} = (2\pi s_x/L, 2\pi s_z/L)$ , leading to:

$$\frac{2\pi N}{Lk} |\sin \theta| \sqrt{(s_x \sin \theta)^2 + (s_z \cos \theta)^2} \lesssim \left( U^3 k_f k^2 \right)^{1/3}. \quad (3.4)$$

The prefactor  $|\sin \theta|$ , implies that the inequality is more likely to be violated at  $\theta \simeq \pm\pi/2$ , i.e. for small wave frequencies  $\omega_{\mathbf{k}} = N \cos \theta$ . Ensuring this condition across all angles  $\theta$  and  $s_x, s_z = 0, \pm 1$  reduces to

$$k \gtrsim \frac{1}{L} (2\pi)^{3/5} (Lk_f)^{-1/5} Fr^{-3/5} \equiv (2\pi)^{3/5} (Lk_f)^{-1/5} k_c, \quad (3.5)$$

where

$$k_c \equiv Fr^{-3/5}/L. \quad (3.6)$$

For a constant  $Lk_f \sim 1$ , we expect the interaction to be concentrated on discrete sets of modes with slow wave frequencies and wave vectors modulus  $k \lesssim k_c$ , leading to discrete wave turbulence (L'vov & Nazarenko 2010). For observing a weak wave turbulence range in the energy spectra, one needs to satisfy

$$k_d \gtrsim k_c \Rightarrow Re_n \gtrsim \left[ (2\pi)^{3/5} (Lk_f)^{-1/5} \right]^{2n-1} Fr^{-(6n-3)/5}, \quad (3.7)$$

Otherwise, the fluid is expected to be in a discrete wave turbulence regime. This observation is crucial for laboratory experiments interested in the weak wave turbulence regime. As our numerical results show in the next section,  $k_c$  plays an important role in strongly stratified turbulence. We define  $k_c$  through dimensional analysis, so we expect a numerical prefactor of order unity when comparing it to observations. Analogous conditions to equations (3.3) and (3.7) are also necessary to make comparisons with weak wave turbulence theory for quantum fluids (Zhu *et al.* 2022), surface waves (Falcon & Mordant 2022), and other systems.

In stratified turbulence, the Ozmidov wave vector  $k_O \equiv \sqrt{N^3/\varepsilon} = (Lk_f)^{-1/2} Fr^{-3/2}/L$ , where

the nonlinear time matches  $N$ , and the Kolmogorov wave vector  $k_\eta \equiv (\varepsilon/\nu_n^3)^{1/(6n-2)} = (Lk_f)^{1/(6n-2)} Re_n^{3/(6n-2)}/L$  are often used. For our simulations, we found it convenient to use  $k_d$  instead of  $k_\eta$  to set the hyper-viscosity for having well-resolved simulations. Yet,  $k_d/k_\eta = (Lk_f)^{-1/(6n-2)} Re_n^{1/(2n-1)(6n-2)}$  so  $k_\eta \simeq k_d$  over the parameter range we investigated. Thus, using  $k_\eta$  instead of  $k_d$  as the dissipative scale would not significantly alter conditions (3.3) and (3.7).

Finally, our analysis assumes that  $U$  is determined solely by the input parameters  $\varepsilon$  and  $k_f$ . The observed deviations of the rms velocity in our simulations are discussed in section 5. In this section, we also connect our “naive” definitions to standard definitions used in studies of stratified flows, using an approximation of the rms velocity based on the discrete wave regime.

## 4. Simulations

### 4.1. Numerical methods

We perform forced-dissipated DNS of equations (2.6-2.7) in a square periodic domain of size  $L = 2\pi$  using a pseudo-spectral method with a standard 2/3 rule for dealising. For the white noise forcing (2.15) we set

$$[k_{f,\min}, k_{f,\max}] = [0.9; 5.1] \Rightarrow k_f = \frac{k_{f,\min} + k_{f,\max}}{2} = 3 \quad \text{and} \quad \varepsilon = 10^{-3}. \quad (4.1)$$

For time advancement, we employ the fractional-step splitting method (McLachlan & Quispel 2002). Namely, we apply the linear operator for a time increment  $dt/2$ , compute the contribution of the nonlinear term using the Runge-Kutta 2 method, and apply the linear operator for  $dt/2$ . This method has the advantage of treating the linear terms explicitly and achieving second-order precision. We denote by  $M$  the number of grid points in each direction. The hyperviscosity order is set to  $n = 4$  and the hyperviscosity  $\nu_n$  is fixed such that the ratio between the maximal wave vector modulus  $k_{\max} = M/3$  and the viscous wave vector  $k_d$  (3.2) is 1.5. The time step  $dt$  is the minimum between  $10^{-2}/N$  and the time step given by a CFL number 0.65. These choices allow us to obtain well-resolved simulations for the investigated range of parameters.

### 4.2. Setting up the data set

To construct our dataset, we first run simulations at a small resolution  $M = 128$ . We start simulations with  $M \geq 256$  from the end of the simulation at the same  $N$  with lower resolution  $M/2$  and decrease the viscosity as we increase the resolution. It allows us to save computational time and reach statistically steady states faster. The simulation time of the small resolution simulations, i.e.  $M = 128$ , is  $\propto 400N$ . For the other simulations, i.e.  $M \geq 256$ , the simulation time is  $\propto 200N$ . Then, our runs are much longer than the kinetic time, which is necessary to reach a statistically steady state of weak internal gravity wave turbulence. We give the list of the simulations, with the values of the relevant parameters, in Tab. 1.

## 5. Study of the flow regimes

We present our simulations on the parametric  $(Fr, Re_n)$  plane and the transition lines for the expected regimes in Fig. 1(a). In Fig. 1(b) We plot the ratio between the r.m.s velocity  $U_{\text{rms}} = \sqrt{2E_{\text{kin}}}$  and the “naive” velocity scale  $U = (\varepsilon/k_f)^{1/3}$ , where  $E_{\text{kin}}$  is the total kinetic energy. This ratio decreases like  $Fr^{-2/5}$ , and is weakly dependent on  $Re_n$ .

### 5.1. Vorticity structure across Regimes

In Fig. 2, we present the vorticity field in the statistically steady state for four simulations. When stratification is weak ( $Fr$  is large) and moderate Reynolds number  $Re_n$ , we observe 2D vortices

$M$	$N$
128	1, 2, 4, 8, 16, 32
256	1, 2, 4, 8, 16, 32
512	1, 2, 4, 8, 16
1024	1, 2, 4, 8, 16
2048	1, 2, 4, 8

Table 1: List of our simulations with relevant control parameters. We set  $L = 2\pi$ ,  $n = 4$ ,  $\varepsilon = 10^{-3}$ ,  $k_f = 3$ , and  $k_{\max}/k_d = 1.5$ . Therefore, the dimensionless parameters (3.1) are then given by  $Fr = 1/[(3000)^{1/3}2\pi N]$  and  $Re_n = (4\pi M/9)^7$ .

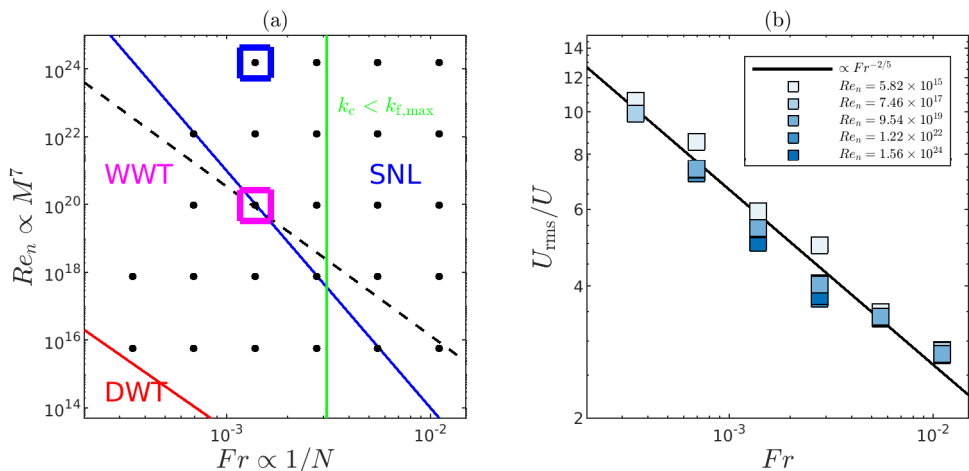


Figure 1: (a) Simulations grid on the parametric plane  $(Fr, Re_n)$ . The blue line represents  $k_b = k_d$  (3.3), which separates the weak wave turbulence from the strong nonlinear regimes. The red line indicates  $k_c = k_d$  (3.7), distinguishing the weak wave turbulence from the discrete wave turbulence regimes. The dashed line corresponds to the transition (5.9), with  $\alpha = 10$ . The green line represents  $k_c = k_{f,\max}$ . The blue box highlights the simulation whose spectra are shown in Fig.4. The magenta box indicates the simulation whose spectra are shown in Fig.6. (b) Ratio between the r.m.s velocity  $U_{\text{rms}}$  and the “naive” velocity scale  $U = (\varepsilon/k_f)^{1/3}$  as a function of  $Fr$  for all simulations with varying  $Re_n$ . The dashed line corresponds to the theoretical scaling (5.2).

without layering (Fig.2(a)). As  $Re_n$  increases, smaller vortices appear (Fig.2(b)), as expected due to the extension of the inertial range. With stronger stratification (smaller  $Fr$ ) we observe layering in the vorticity field (Fig.2(c)). This phenomenon has been reported previously in simulations without shear modes (Calpe Linares 2020). Notably, the layers’ thickness remains unchanged after further increases in  $Re_n$ ; while the vortices become smaller (Fig.2(d)).



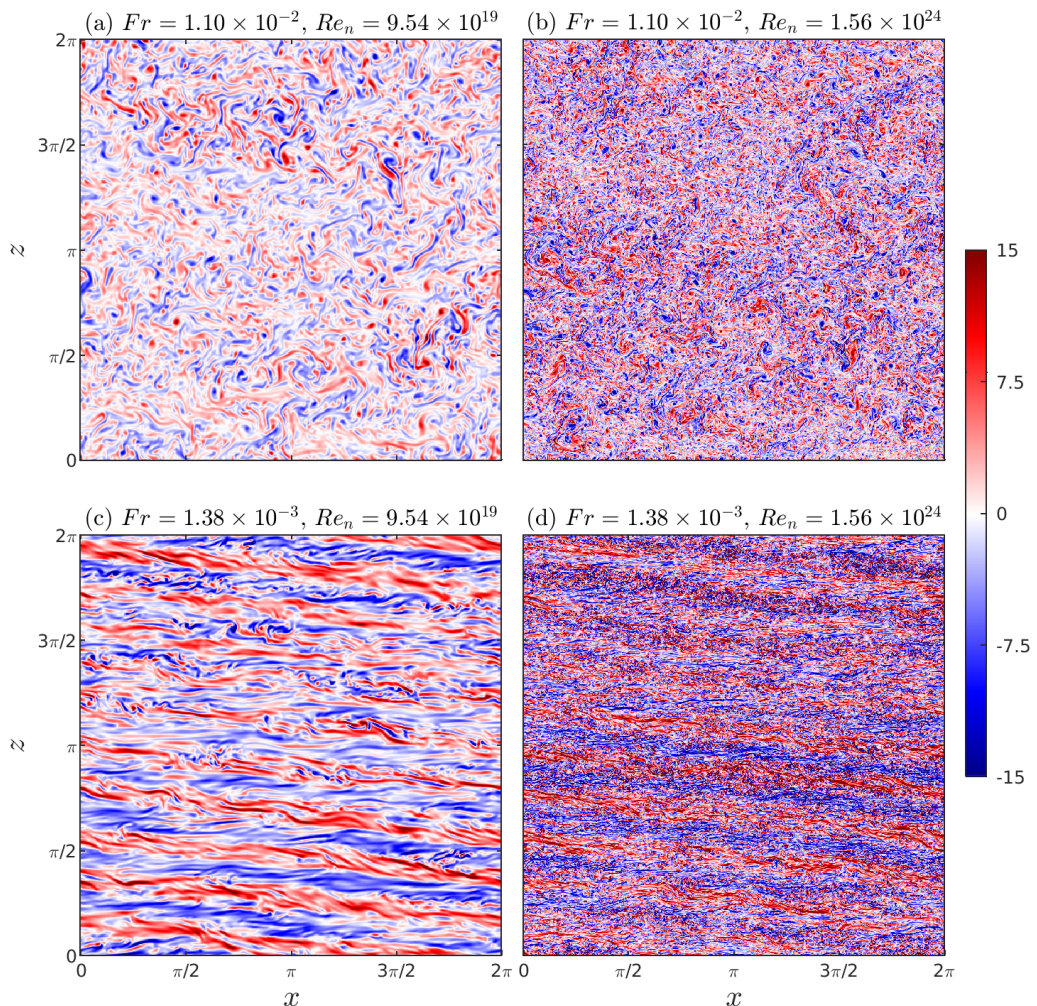


Figure 2: Vorticity field in the statistically steady state for simulations with different  $Fr$  and  $Re_n$ .

### 5.2. Energy spectra across regimes

In Fig.3, we present the compensated 1D spectra

$$e(k) = \sum_{\mathbf{k}', k-1 \leq k' < k} e(\mathbf{k}) \quad (5.1)$$

for four simulations across various regimes: (a) strong nonlinear - weakly stratified regime, (b) strong nonlinear - strongly stratified regime, (c) weak wave turbulence, and (d) discrete wave interaction.

When the stratification is weak and the nonlinearity is strong (a), the potential energy spectrum differs from the kinetic energy spectrum, particularly for  $k > k_O$ . In this case, the spectra are continuous, except at the end of the forcing range. As stratification increases (b), both  $k_b$  and  $k_O$  become larger, leading to closer alignment between the kinetic and potential energy spectra across a broader range. In this simulation, nearly all energetic scales are influenced by stratification, as  $k_O \simeq k_\eta$ . In the weak wave turbulence regime (c), characterised by intermediate stratification and nonlinearity, we satisfy condition (3.3) so all energetic scales are expected to interact through

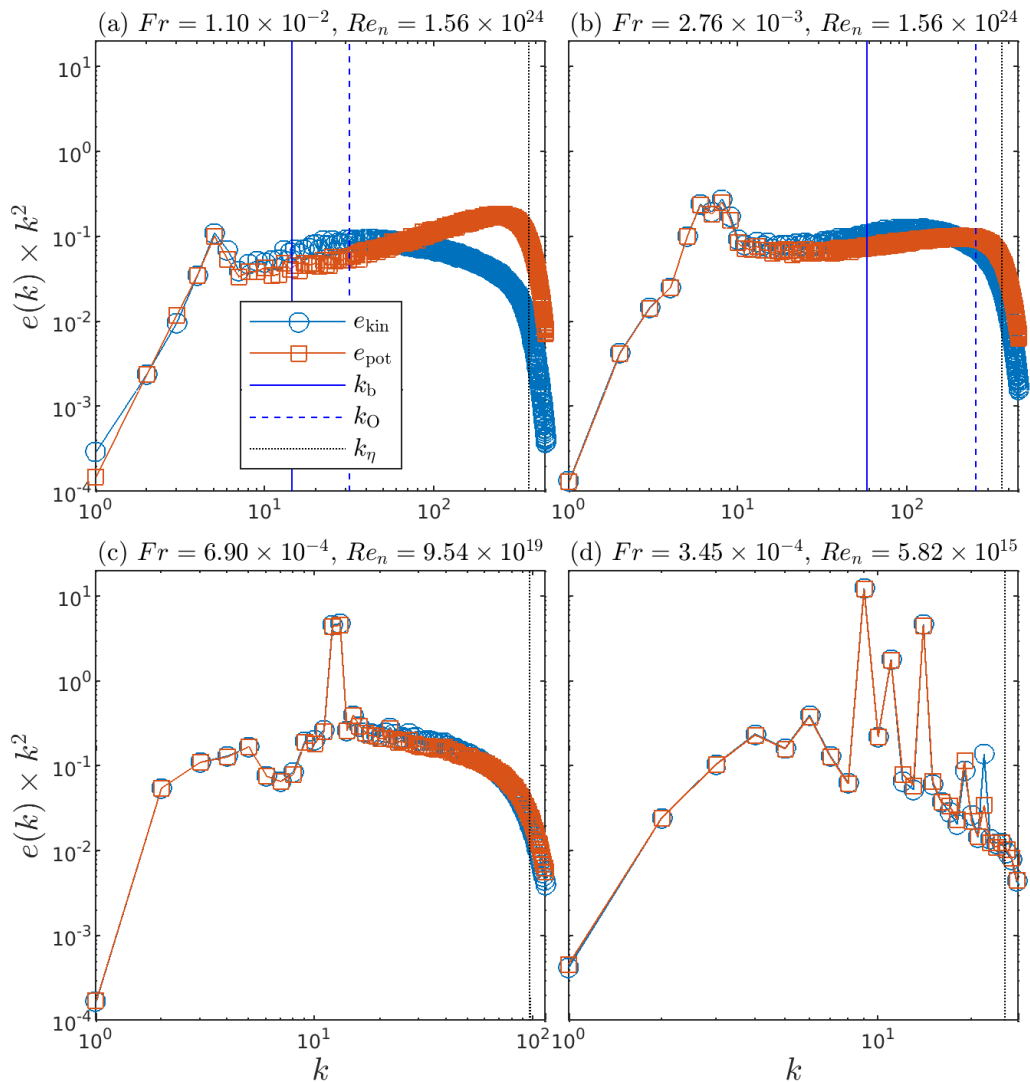


Figure 3: 1D kinetic and potential energy spectra for four simulations, compensated by  $k^2$ . Vertical lines correspond to buoyancy, Ozmidov, and Kolmogorov wave vectors  $k_b$ ,  $k_O$ , and  $k_\eta$ . For each panel, we show only the range  $k \in [1 : k_d]$ , which contains almost all the energy.

weak nonlinearity. The potential and kinetic energy spectra are nearly equal across all scales, which is typical for internal gravity waves. Yet, the energy spectrum peaks around  $k = 13$ , with only the range  $k \gtrsim 13$  appearing continuous. The peak, which corresponds to the layering, also perturbs the scaling for large wave vectors  $k \gtrsim 13$  and we do not observe the theoretical scaling in this simulation. For the simulation in panel (d), the stratification is the highest, and nonlinearity is the weakest such that condition (3.7) is almost violated. In this regime, energetic scales interact predominantly through a discrete set of interactions, as evidenced by the numerous discrete peaks in the spectrum. It confirms that the simulation corresponds to the discrete wave interaction regime.

### 5.3. Strong non linearity regime

In Fig.4(a-b), we show slices of the energy spectra at various frequencies as a function of the wave vector amplitude  $k$ , compensated by the weak wave turbulence prediction (1.1), for a simulation in the strong nonlinearity regime. We see in panel (a) that the kinetic energy spectrum is shallower than  $k^{-3}$  and has a maximum at  $k = k_b$  and high  $\omega_k$ , as observed in earlier studies (see e.g. Waite (2011); Augier *et al.* (2015)). For slow frequencies  $\omega_k/N = 0.1$  we observe a peak at the critical wave vector  $k \simeq k_c$  corresponding to layering. It indicates that  $k_c = Fr^{-3/5}/L$ , obtained using weak wave turbulence theory in section 3, is relevant for strongly stratified flows beyond the weakly nonlinear regime. The potential energy spectrum, shown in panel (b), follows the same trends with a less pronounced maximum at  $k = k_b$ .

In panel (c), we show the energy transfers (2.13):

(i) For  $k \lesssim k_c$ , the transfers  $\mathcal{T}_{\text{kin}}$  and  $\mathcal{T}_{\text{pot}}$  have no clear behavior, with a sharp transition around  $k_c$ ;

(ii) For  $k \in [k_c, k_b]$ , the transfers have clear tendencies. Potential energy goes forward (to small scales) while converted to kinetic energy, and the kinetic goes backward (to large scale) and is converted back to potential energy. The total energy transfer equals the average injection rate  $\varepsilon$ . Interestingly, this picture is consistent with the energy cycle explained in Müller *et al.* (1986) (see Figs.27 and 28 of this reference).

(iii) In the range  $k \in [k_b, k_\eta]$ ,  $\mathcal{T}_{\text{pot}}$  decreases and  $\mathcal{T}_{\text{kin}}$  increases such that both are positive, and their sum is still  $\varepsilon$ .

(iv) At  $k \simeq k_\eta$ ,  $\mathcal{T}_{\text{kin}}$  and  $\mathcal{T}_{\text{pot}}$  decrease to zero. The transfers are negligible only when  $k \simeq k_d$ , and it is tempting to interpret the range  $k \in [k_\eta, k_d]$  as an ‘‘intermittent’’ range. Yet, the smallness of this range does not allow it to be conclusive.

In panel (d), we show the energy transfers (2.14) as a function of  $|\omega_k|/N = |\cos \theta|$ .  $\mathcal{T}_{\text{kin}}$  and  $\mathcal{T}_{\text{pot}}$  are non-monotonous and have opposing trends. At low wave frequencies, the kinetic energy goes to smaller  $\omega_k$  and the potential energy to larger  $\omega_k$ . It explains the layering observed in the vorticity field for slow waves at low  $Fr$  (Fig.2(c-d)). The total energy transfer is positive for all wave frequencies meaning that the total energy transfer is toward higher  $\omega_k$ .

### 5.4. Layering

We explain the layering in our strongly stratified simulations as follows: The potential energy goes forward in scale and is converted into kinetic energy that goes backward in scale; The backward kinetic energy cascade stops at  $k \simeq k_c$  due to the discreteness of the wave-wave interactions so energy accumulates at this scale; Since the condition (3.4) is more easily broken at small wave frequencies, we expect the energy accumulation to be for small  $\omega_k$ .

If the inverse energy transfers stop at  $k \simeq k_c$ , a mechanism must act against the accumulation of kinetic energy. Otherwise, simulations of 2D stratified turbulence without shear modes would not reach a statistically steady state, as observed here and in Calpe Linares (2020). One possible mechanism is that the energy carried by the inverse kinetic transfers is converted to potential energy at  $k \simeq k_c$ . An order of magnitude estimate of equations (2.2-2.3) yields the large scale flow velocity  $U_L$ :

$$|\mathbf{u} \cdot \nabla \mathbf{u}| \sim |b| \quad \Rightarrow \quad U_L^2 k_c \sim NU_L \quad \Rightarrow \quad U_L \propto \frac{N}{k_c} = UFr^{-2/5}, \quad (5.2)$$

where we have used  $|b| \sim NU_L$  and (3.6). This mechanism is impossible for shear modes, which have zero vertical velocity. It may explain why strongly stratified simulations with shear modes take a much longer time to reach a steady state (Smith 2001; Smith & Waleffe 2002) (see also (Brethouwer *et al.* 2007) and references therein). When shear modes are present, the steady state is reached after several instabilities (Caulfield 2021), leading to the increase of the layers’ thickness and large-scale flow velocity (Rommel *et al.* 2014; Fitzgerald & Farrell 2018a). We can also

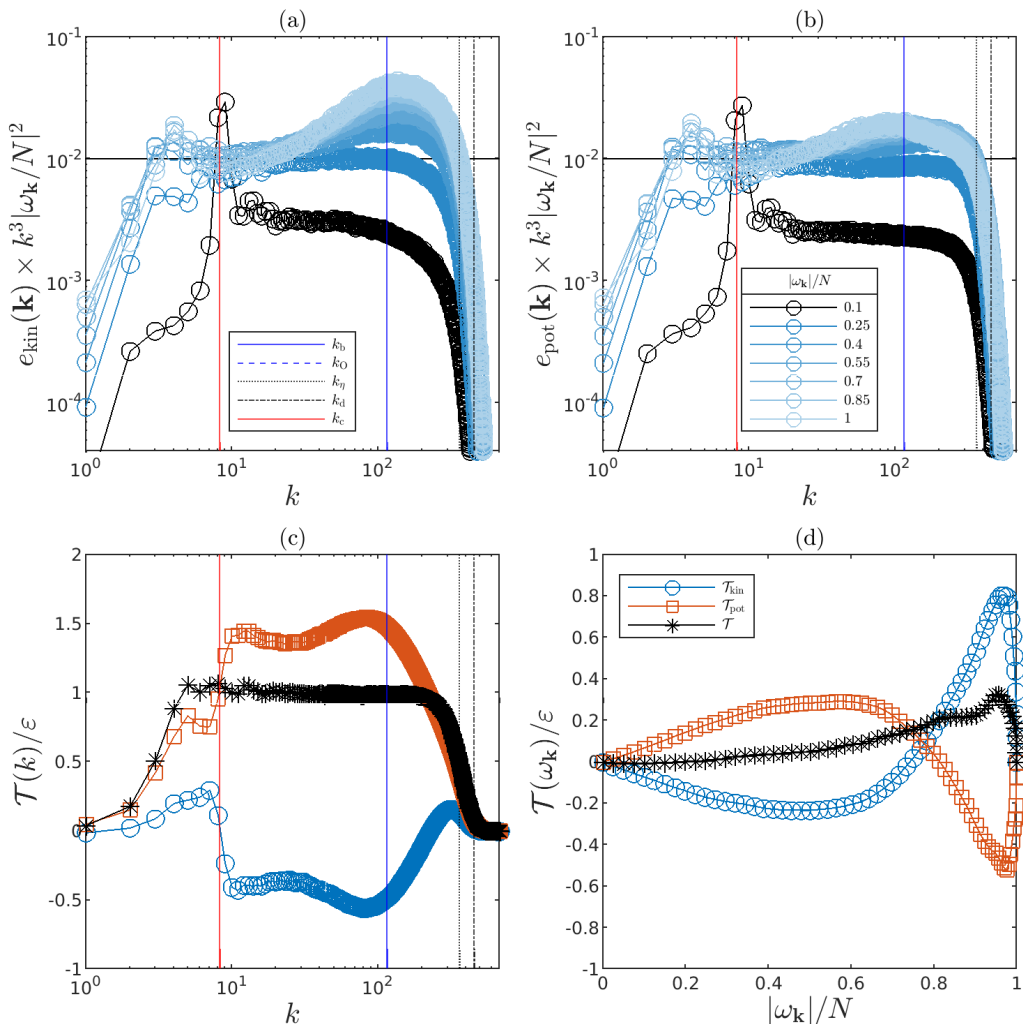


Figure 4: Energy spectra and energy transfers for the simulation in the strong nonlinear regime with  $Fr = 1.38 \times 10^{-3}$  and  $Re_n = 1.56 \times 10^{24}$ . (a) Slices of the compensated kinetic energy spectrum and (b) slices of the compensated potential energy spectrum for different wave frequencies. (c) Normalised energy transfers as a function of  $k$ . (d) Normalised energy transfers as a function of  $|\omega_{\mathbf{k}}|/N$ . Legend in panel (a) is used for panels (b) and (c), legend in panel (b) is used for panel (a), and legend in panel (d) is used for panel (c).

obtain the scaling (5.2) by assuming that the flow reaches a critical Richardson number. Namely, using the estimate  $|\partial_z \langle u_x \rangle| \sim k_c U_L$ , we can write

$$Ri \equiv \frac{N^2}{(\partial_z \langle u_x \rangle)^2} = Ri_c = \text{constant} \quad \Rightarrow \quad U_L \propto \frac{N}{k_c} = UFr^{-2/5}. \quad (5.3)$$

The two reasoning (5.2) and (5.3) mean that the vertical Froude number based on  $L_z = 2\pi/k_c$  and  $U_L$ , namely  $Fr_z^* = U_L/(NL_z)$ , is of order unity. It is therefore consistent with earlier studies (Billant & Chomaz 2001; Brethouwer *et al.* 2007). For our simulations, where layering is present,  $U_{\text{rms}} = \sqrt{2E_{\text{kin}}}$  is close to the large scale flow velocity  $U_L$ . We observe in Fig.1(b) that the expected scaling (5.2) is verified. Therefore, the relation (5.2) gives a first-order estimate of the

typical velocity of 2D stratified flows when shear modes are removed, at least for  $Fr$  and  $Re_n$  investigated here.

It allows us to define the turbulent Froude and (hyper-viscous) Reynolds numbers (Brethouwer *et al.* 2007)

$$Fr^* \equiv \frac{\varepsilon}{NU_L^2} = (Lk_f) Fr^{9/5} \quad \text{and} \quad Re_n^* \equiv \frac{U_L^{6n-2}}{\nu_n \varepsilon^{2n-1}} = (Lk_f)^{1-2n} Re_n Fr^{(-12n+4)/5} \quad (5.4)$$

that are based on  $U_L \propto U_{\text{rms}}$ . Note that the turbulent Froude number is much lower than  $Fr$  and the turbulent Reynolds number much larger than  $Re_n$  for small  $Fr$  and large  $Re_n$ . We can also compute the associated buoyancy wave vector and the viscous wave vector as follows

$$k_b^* \equiv \frac{Fr^*}{L} \quad \text{and} \quad k_d^* \equiv \frac{Re_n^{*1/(2n-1)}}{L}. \quad (5.5)$$

Equations (5.4-5.5) link our naive definitions (3.1-3.2) with the definitions widely used in other studies of stratified flows, as far as the scaling (5.2) is valid.

### 5.5. Verification of the weak wave turbulence prediction

Weak wave turbulence means that, though non-linearly interacting, the linear waves remain the main degrees of freedom and carry most of the energy (Le Reun *et al.* 2017, 2018; Yokoyama & Takaoka 2019; Lam *et al.* 2020)). It can be easily verified through the spatiotemporal energy spectrum, that is the Fourier transform in time of the energy spectral density:

$$e(\mathbf{k}, \omega) = \frac{k^2 |\hat{\psi}_{\mathbf{k}}(\omega)|^2}{2} + \frac{|\hat{b}_{\mathbf{k}}(\omega)|^2}{2N^2}, \quad (5.6)$$

where  $\hat{\psi}_{\mathbf{k}}(\omega)$  and  $\hat{b}_{\mathbf{k}}(\omega)$  are the Fourier transform in time of  $\hat{\psi}_{\mathbf{k}}(t)$  and  $\hat{b}_{\mathbf{k}}(t)$ . Physically,  $e(\mathbf{k}, \omega)$  is the energy density at wave vector  $\mathbf{k}$  and temporal frequency  $\omega$ . If the flow is of weakly nonlinear waves, we expect  $e(\mathbf{k}, \omega) \sim \delta(\omega \pm \omega_{\mathbf{k}})$ . Otherwise, strong nonlinear interactions or other flow modes are important (Nazarenko 2011).

In Fig.5, we show the spatiotemporal energy spectrum as a function of  $\omega_{\mathbf{k}}$  and  $\omega$  for four simulations, obtained after a straightforward summation over  $\mathbf{k}$ . To compute this spectrum, we use modes with  $|\mathbf{k}| \leq M/4 < k_{\text{max}}$  to save computational time. Since these modes contain most of the energy, this truncation has little impact on the results. For weak stratification, the energy is not only on the linear dispersion relation curve, as shown in Fig.5(a-b). For a simulation at higher stratification, shown in panel (c), we see that most of the energy is concentrated near the linear dispersion relation, meaning that this simulation is more likely to meet weak wave turbulence assumptions. We will use this simulation to compare the energy spectra to the theoretical prediction.

In Fig.6(a-b), we show slices of the kinetic and potential energy spectra, compensated by the weak wave turbulence prediction (1.1), for the simulation with  $Fr = 1.38 \times 10^{-3}$  and  $Re_n = 9.54 \times 10^{19}$ . We see a good agreement between the theory and our DNS, except for low frequencies  $\omega_{\mathbf{k}}/N$  where the spectral peak due to layering is present. Also, the potential energy spectrum decreases faster than the kinetic energy spectrum, particularly at high  $\omega_{\mathbf{k}}/N$ , because the potential energy is ‘‘taxed’’ by the conversion to potential energy while transferred to small scales. We see in Fig.6(c-d) that the energy transfers are similar to the simulation with larger  $Re_n$  (Fig.4)(c-d), except that there is less inertial range and  $k_d \simeq k_b$  so we do not observe the bump at  $k = k_b$ . To our knowledge, it is the first verification of the theoretical prediction for weak non-hydrostatic internal gravity waves.



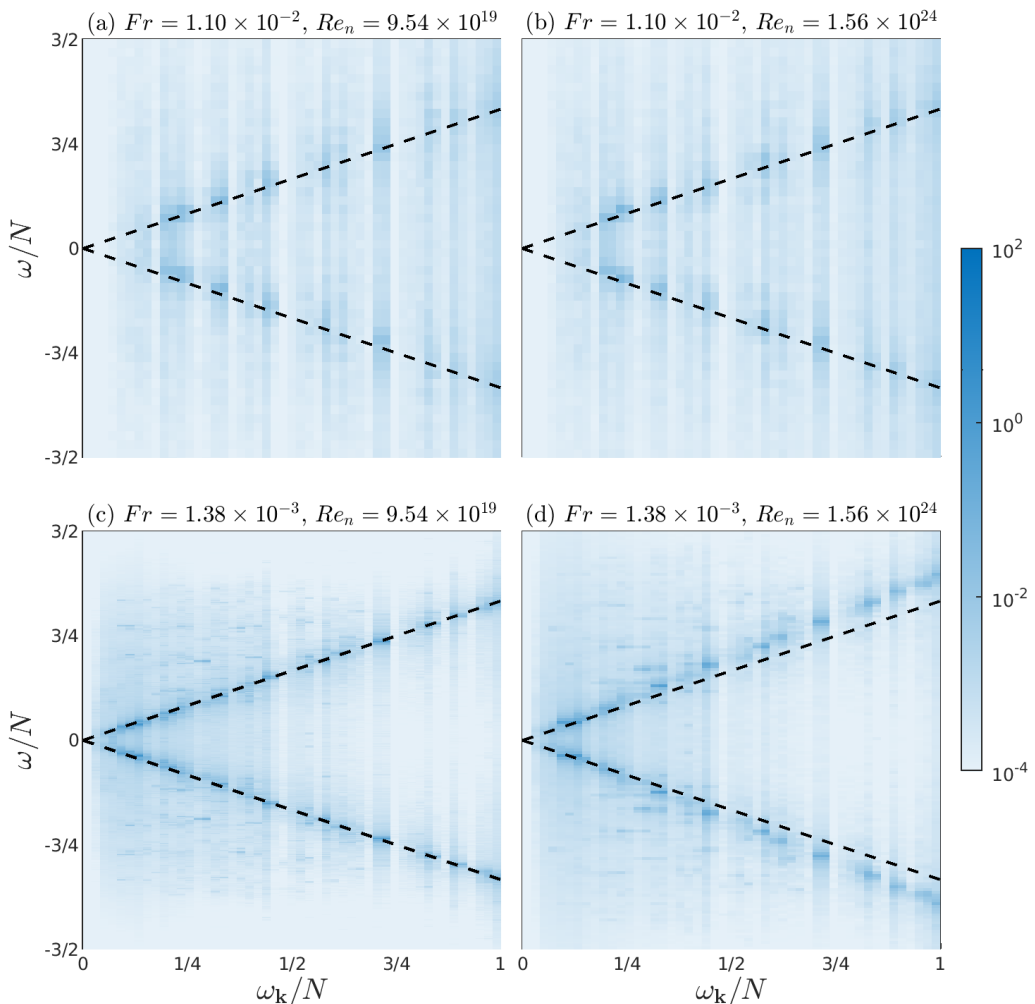


Figure 5: Spatiotemporal energy spectrum  $e(\omega_k, \omega)$  for four of our simulations. In all panels, the dashed lines correspond to the dispersion relation  $\omega = \pm\omega_k$ .

### 5.6. Doppler shift

Keeping stratification high and increasing the nonlinearity compared to the weak wave turbulence simulation, we see that the spatiotemporal spectrum gets a shift from the dispersion relation  $\omega = \pm\omega_k$ , visible in Fig.5(d). This Doppler shift is known to occur in rotating and/or stratified flows due to the nonlinear interactions with the large-scale flow (see e.g. (Clark di Leoni & Mininni 2015; Campagne *et al.* 2015; Lam *et al.* 2020)). To quantify this Doppler shift, we compare the linear wave frequency to the empirical frequency

$$\omega_{\text{emp}}(\omega_k) = \frac{\sum_{\omega} \omega e(\omega_k, \omega)}{\sum_{\omega} e(\omega_k, \omega)}. \quad (5.7)$$

In Fig.7, we show  $\omega_{\text{emp}}$  as a function of  $\omega_k$  for all our simulations. Panel (a) corresponds to weak stratification  $Fr = 1.10 \times 10^{-2}$ . In this case,  $\omega_{\text{emp}}/N$  is close to unity for all wave frequencies, meaning that energy is not on the linear dispersion relation. The empirical frequency depends weakly on the Reynolds number. In panel (b), for  $Fr = 5.52 \times 10^{-3}$ ,  $\omega_{\text{emp}}$  gets closer

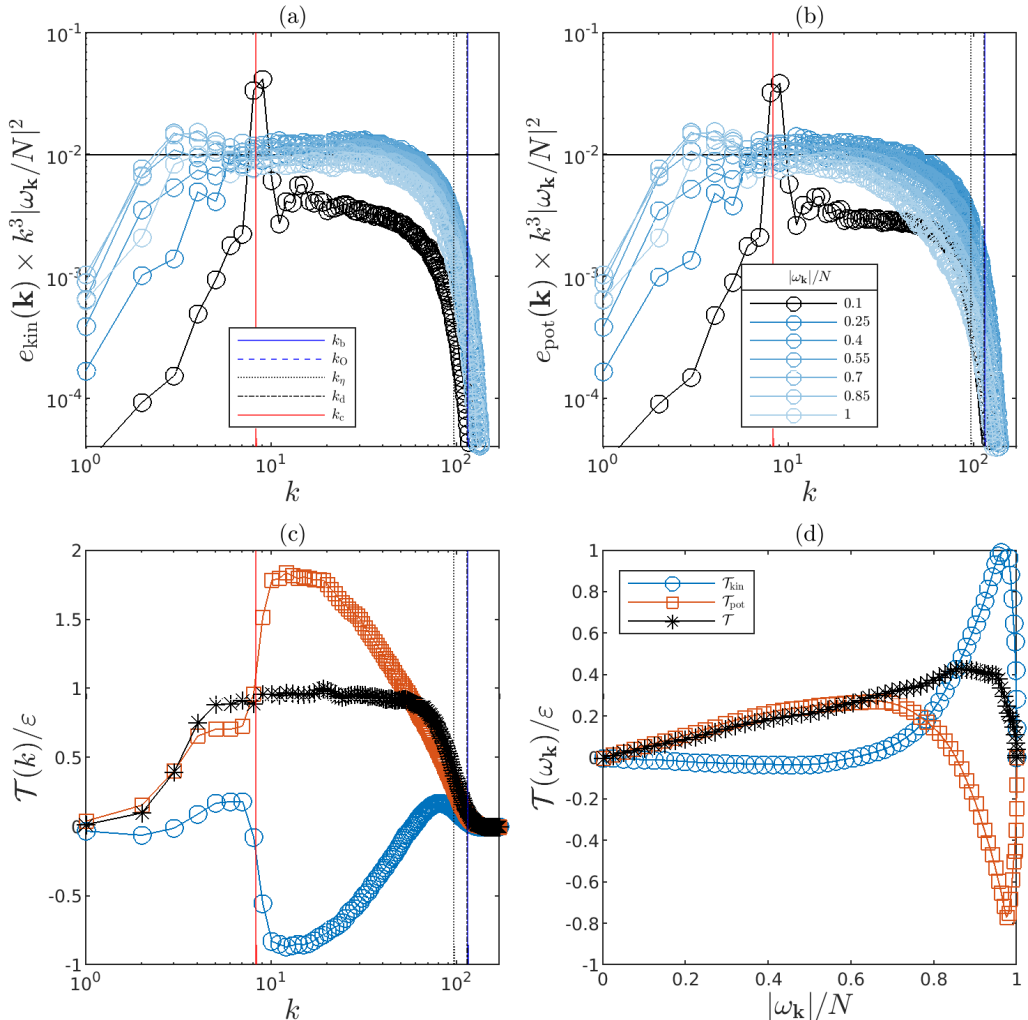


Figure 6: Energy spectra and energy transfers for the simulation with  $Fr = 1.38 \times 10^{-3}$  and  $Re_n = 9.54 \times 10^{19}$ , in the weak wave turbulence regime. (a) Slices of the compensated kinetic energy spectrum and (b) slices of the compensated potential energy spectrum for different wave frequencies. (c) Normalised energy transfers as a function of  $k$ . (d) Normalised energy transfers as a function of  $|\omega_k|/N$ . Legend in panel (a) is used for panels (b) and (c), legend in panel (b) is used for panel (a), and legend in panel (d) is used for panel (c).

to the wave dispersion relation for higher  $\omega_k$  and still has a weak dependence on  $Re_n$ . In panel (c), for  $Fr = 2.76 \times 10^{-3}$ ,  $\omega_{\text{emp}}$  is close to  $\omega_k$  except at small wave frequencies. We do not observe the Doppler shift for weak stratification at  $Fr > 2.76 \times 10^{-3}$  when  $k_c$  is less or close to  $k_{f,\text{max}}$  (see Fig. 1(a)). This observation is in line with Clark di Leoni & Mininni (2015), who explained that the layering process requires external forcing not to disrupt the development of the large-scale flow. In panel (d-f), for  $Fr \leq 1.38 \times 10^{-3}$ , we observe different behavior depending on the Reynolds number. For lowest  $Re_n$ ,  $\omega_{\text{emp}}$  gets closer to  $\omega_k$  as the increases. On the contrary, for the highest  $Re_n$ , we observe a significant shift in  $\omega_{\text{emp}}$ . The Doppler shift is visible for three simulations: ( $Fr = 1.38 \times 10^{-3}$ ,  $Re_n = 1.22 \times 10^{22}$ ), ( $Fr = 1.38 \times 10^{-3}$ ,  $Re_n = 1.56 \times 10^{24}$ ) and

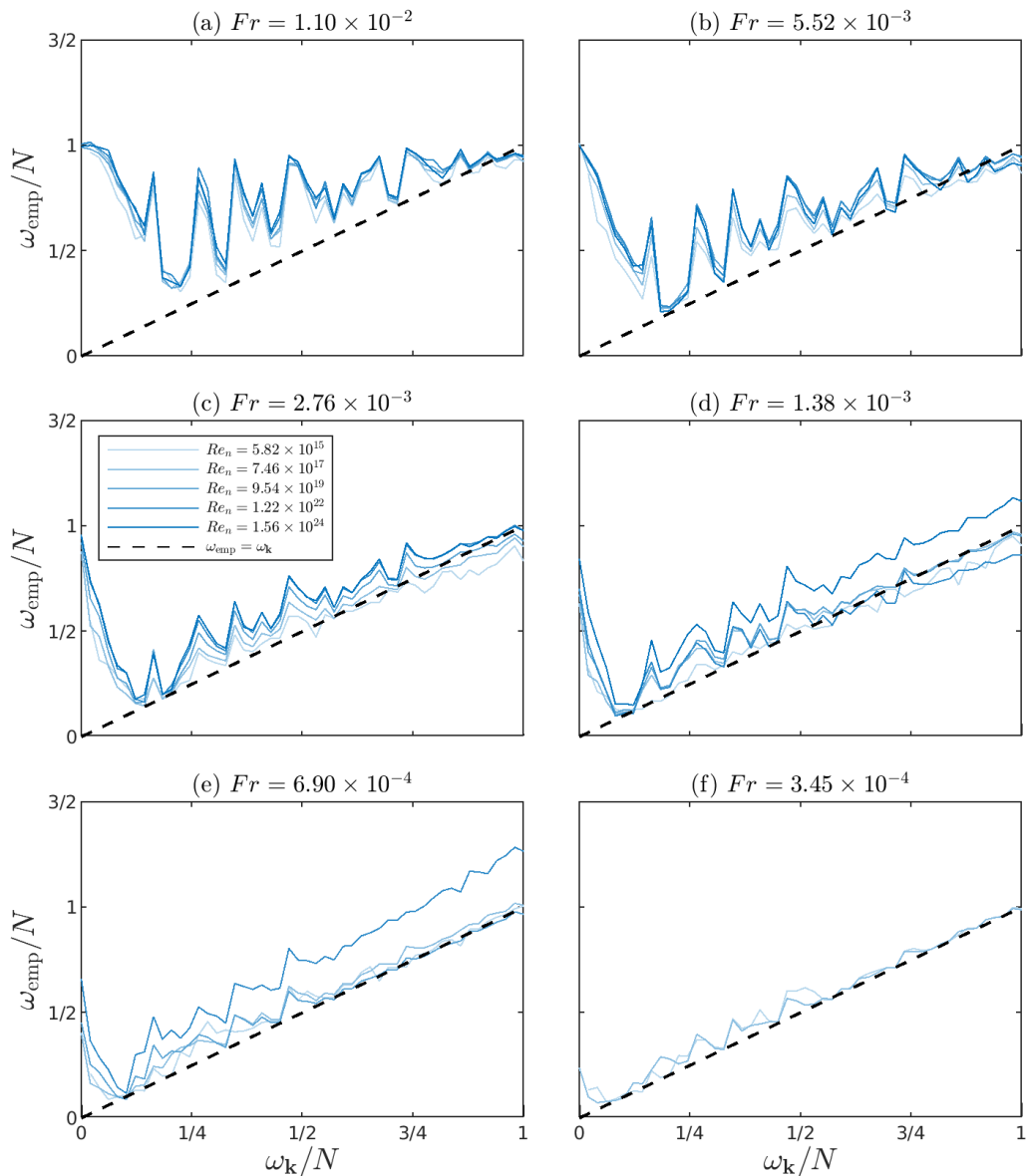


Figure 7: Empirical frequency (5.7) vs the wave frequency  $\omega_k$  for all our simulations. In all panels, the dashed line indicates  $\omega_{\text{emp}} = \omega_k$ .

( $Fr = 6.90 \times 10^{-4}$ ,  $Re_n = 1.22 \times 10^{22}$ ), shown in panels (d-e). It prevented us from using these simulations to compare weak wave turbulence predictions for the energy spectrum.

It is known that the Doppler shift appears when the sweeping frequency due to the large scale flow becomes larger than the linear frequency (see e.g. Clark di Leoni & Mininni (2015)). For our simulations, it yields to the condition

$$U_L k \gtrsim N. \quad (5.8)$$



If we want it to be valid in the inertial range, namely  $k \lesssim k_\eta \propto Re_n^{3/6n-2}/L$ , it follows that

$$UFr^{-2/5} \frac{Re_n^{3/6n-2}}{L} \gtrsim \alpha N \quad \Rightarrow \quad Re_n \gtrsim \alpha^{(6n-2)/3} Fr^{(2-6n)/5}, \quad (5.9)$$

where we have used (5.2) and  $\alpha$  is an undetermined numerical constant. The physical meaning of (5.9) is that the mean flow starts to create frequencies bigger than  $N$ , that are not damped by viscosity. In Fig. 1(b), we show the line given by condition (5.9) with  $\alpha = 10$ . The simulations affected by the Doppler shift are above this line and for  $k_c > k_{f,\max}$ .

## 6. Conclusions and discussions

We performed direct numerical simulations of 2D stratified turbulence without shear modes (also called Vertically Sheared Horizontal Flows). In the weak wave turbulence regime, we verified the theoretical predictions outside the hydrostatic limit (Shavit *et al.* 2024). The energy spectrum agrees with the theory except for low wave frequencies. Yet, our simulations are subject to layering -an accumulation of energy in slow waves- which perturbs the theoretical predictions. This layering occurs also outside the weakly nonlinear regimes, as observed in many earlier studies (Smith & Waleffe 2002; Laval *et al.* 2003; Waite 2011; Rempel *et al.* 2014; Fitzgerald & Farrell 2018a; Calpe Linares 2020).

We explain the layering by the inverse kinetic energy transfers and the discreteness of the wave-wave interactions at large scales, typical of weakly nonlinear wave systems (Nazarenko 2011). It allows us to obtain quantitative predictions for the layers' thickness  $L_z$  and the large-scale velocity  $U_L$ , using only the input parameters of the simulations. These predictions agree with our simulations, even outside the weakly nonlinear regime. It is also consistent with the idea that the flow selects  $L_z$  and  $U_L$  such that the vertical Froude number  $U_L/(NL_z)$  is of order unity (Billant & Chomaz 2001). For strongly stratified simulations at large Reynolds numbers, we observe that the measured wave frequency is impacted by a Doppler shift, commonly observed in stratified and rotating flows (Clark di Leoni & Mininni 2015; Campagne *et al.* 2015; Lam *et al.* 2020).

2D stratified turbulence with shear modes, and 3D stratified turbulence are naturally more complex than the idealized simulations presented in this study because other instabilities can occur (Caulfield 2021). Yet, we expect our order of magnitude to be relevant for discussing some transitions of strongly stratified turbulence. In particular, the layering and the Doppler shift are absent from our simulation when the random forcing perturbs the layering because  $k_c \lesssim k_{f,\max}$  lies in the forcing range. This behavior, together with our estimate  $k_c \propto Fr^{-3/5}/L$ , may help to explain the emergence of layering in realistic flows and the discrepancies between simulations/experiments employing different setups. It is tempting to apply our argument to rotating flows without geostrophic modes. In that context,  $k_c = Ro^{-3/5}/L$  where  $Ro = U/(\Omega L)$  is the Rossby number and  $\Omega$  the rotation rate. In that context,  $L_h = 2\pi/k_c$  would correspond to the radius of nearly vertical columnar flows.

For observing weak wave turbulence of internal waves, one must ensure that the large-scale flow, whose size is fixed by discrete wave turbulence Nazarenko (2011), is destroyed. It can be done by adding large-scale damping (Le Reun *et al.* 2017; Brunet *et al.* 2020), or by using a random forcing over the all discrete turbulence range  $k \lesssim k_c$ . Another way of preventing the formation of large scale would be to use a large aspect ratio so the large scale flow cannot exist in the simulation box or the container. Interestingly, considering an asymptotic limit of the Navier-Stokes equations, van Kan & Alexakis (2020, 2022) identified transitions to large-scale flow formations for critical values of the aspect ratio. Yet, as explained by the authors, their asymptotic is different from weak wave turbulence and is unlikely to be directly related to the present work.

**Acknowledgements.** We thank Giorgio Krstulovic for providing the structure for the code used in this work

together with endless advice; Oliver Bühler, Sergey Nazarenko, Jalal Shatah, Gregory Falkovich, Pierre Augier, Paul Billant, and Colm-cille Caulfield for fruitful discussions.

**Funding.** This work was supported by the Simons Foundation and the Simons Collaboration on Wave Turbulence. The numerical study was made possible thanks to New York University’s Greene computing cluster facility. MS acknowledges additional financial support from the Schmidt Futures Foundation.

**Declaration of interests.** The authors report no conflict of interest.

**Author ORCIDs.** V. Labarre, <https://orcid.org/0000-0002-5081-4008>; M. Shavit, <https://orcid.org/0000-0002-7252-7077>

**Author contributions.** Both authors conducted this study, performed the simulations, and wrote the manuscript.

## REFERENCES

- ANDREWS, DAVID G, HOLTON, JAMES R & LEOVY, CONWAY B 1987 *Middle atmosphere dynamics. International Geophysics* 40. Elsevier Science.
- AUGIER, PIERRE, BILLANT, PAUL & CHOMAZ, JEAN-MARC 2015 Stratified turbulence forced with columnar dipoles: numerical study. *Journal of Fluid Mechanics* **769**, 403–443.
- BALMFORTH, N. J., LLEWELLYN SMITH, STEFAN G. & YOUNG, W. R. 1998 Dynamics of interfaces and layers in a stratified turbulent fluid. *Journal of Fluid Mechanics* **355**, 329–358.
- BILLANT, PAUL & CHOMAZ, JEAN-MARC 2000a Experimental evidence for a new instability of a vertical columnar vortex pair in a strongly stratified fluid. *Journal of Fluid Mechanics* **418**, 167–188.
- BILLANT, PAUL & CHOMAZ, JEAN-MARC 2000b Theoretical analysis of the zigzag instability of a vertical columnar vortex pair in a strongly stratified fluid. *Journal of Fluid Mechanics* **419**, 29–63.
- BILLANT, PAUL & CHOMAZ, JEAN-MARC 2001 Self-similarity of strongly stratified inviscid flows. *Physics of Fluids* **13** (6), 1645–1651.
- BOFFETTA, G., LILLO, F. DE, MAZZINO, A. & MUSACCHIO, S. 2011 A flux loop mechanism in two-dimensional stratified turbulence. *Europhysics Letters* **95** (3), 34001.
- BOUROUBA, LYDIA 2008 Discreteness and resolution effects in rapidly rotating turbulence. *Phys. Rev. E* **78**, 056309.
- BRETHOUWER, G., BILLANT, P., LINDBORG, E. & CHOMAZ, J.-M. 2007 Scaling analysis and simulation of strongly stratified turbulent flows. *Journal of Fluid Mechanics* **585**, 343–368.
- BRUNET, MAXIME, GALLET, BASILE & CORTET, PIERRE-PHILIPPE 2020 Shortcut to geostrophy in wave-driven rotating turbulence: the quartet instability. *Physical Review Letters* **124** (12), 124501.
- BUCKMASTER, TRISTAN, GERMAIN, PIERRE, HANI, ZAHER & SHATAH, JALAL 2021 Onset of the wave turbulence description of the longtime behavior of the nonlinear schrödinger equation. *Inventiones mathematicae* **225**, 787–855.
- BÜHLER, OLIVER 2014 *Waves and mean flows*. Cambridge University Press.
- CAILLOL, PH & ZEITLIN, V 2000 Kinetic equations and stationary energy spectra of weakly nonlinear internal gravity waves. *Dynamics of atmospheres and oceans* **32** (2), 81–112.
- CALPE LINARES, MIGUEL 2020 Numerical study of 2D stratified turbulence forced by internal gravity waves. PhD thesis, Université Grenoble Alpes.
- CAMPAGNE, ANTOINE, GALLET, BASILE, MOISY, FRÉDÉRIC & CORTET, PIERRE-PHILIPPE 2015 Disentangling inertial waves from eddy turbulence in a forced rotating-turbulence experiment. *Physical Review E* **91** (4), 043016.
- CAULFIELD, C. P. 2021 Layering, Instabilities, and Mixing in Turbulent Stratified Flows. *Annual Review of Fluid Mechanics* **53** (Volume 53, 2021), 113–145.
- DEMATTEIS, GIOVANNI, LE BOYER, ARNAUD, POLLMANN, FRIEDERIKE, POLZIN, KURT L, ALFORD, MATTHEW H, WHALEN, CAITLIN B & LVOV, YURI V 2024 Interacting internal waves explain global patterns of interior ocean mixing. *Nature Communications* **15** (1), 7468.
- DEMATTEIS, GIOVANNI & LVOV, YURI V. 2021 Downscale energy fluxes in scale-invariant oceanic internal wave turbulence. *Journal of Fluid Mechanics* **915**, A129.
- FALCON, ERIC & MORDANT, NICOLAS 2022 Experiments in surface gravity–capillary wave turbulence. *Annual Review of Fluid Mechanics* **54** (Volume 54, 2022), 1–25.

- FARRELL, BRIAN F. & IOANNOU, PETROS J. 2003 Structural stability of turbulent jets. *Journal of the Atmospheric Sciences* **60** (17), 2101–2118.
- FITZGERALD, JOSEPH G. & FARRELL, BRIAN F. 2018a Statistical state dynamics of vertically sheared horizontal flows in two-dimensional stratified turbulence. *Journal of Fluid Mechanics* **854**, 544–590.
- FITZGERALD, JOSEPH G. & FARRELL, BRIAN F. 2018b Statistical state dynamics of vertically sheared horizontal flows in two-dimensional stratified turbulence. *Journal of Fluid Mechanics* **854**, 544–590.
- GALTIER, SÉBASTIEN 2022 *Physics of Wave Turbulence*. Cambridge University Press.
- GARRETT, CHRISTOPHER & MUNK, WALTER 1979 Internal waves in the ocean. *Annual review of fluid mechanics* **11** (1), 339–369.
- HASSELMANN, KLAUS 1966 Feynman diagrams and interaction rules of wave-wave scattering processes. *Reviews of Geophysics* **4** (1), 1–32.
- HOWARD, LOUIS N. 1961 Note on a paper of John W. Miles. *Journal of Fluid Mechanics* **10** (4), 509–512.
- HOWLAND, CHRISTOPHER J., TAYLOR, JOHN R. & CAULFIELD, C. P. 2020 Mixing in forced stratified turbulence and its dependence on large-scale forcing. *Journal of Fluid Mechanics* **898**, A7.
- VAN KAN, ADRIAN & ALEXAKIS, ALEXANDROS 2020 Critical transition in fast-rotating turbulence within highly elongated domains. *Journal of Fluid Mechanics* **899**, A33.
- VAN KAN, ADRIAN & ALEXAKIS, ALEXANDROS 2022 Energy cascades in rapidly rotating and stratified turbulence within elongated domains. *Journal of Fluid Mechanics* **933**, A11.
- LABARRE, VINCENT, AUGIER, PIERRE, KRSTULOVIC, GIORGIO & NAZARENKO, SERGEY 2024a Internal gravity waves in stratified flows with and without vortical modes. *Phys. Rev. Fluids* **9**, 024604.
- LABARRE, VINCENT, LANCHON, NICOLAS, CORTET, PIERRE-PHILIPPE, KRSTULOVIC, GIORGIO & NAZARENKO, SERGEY 2024b On the kinetics of internal gravity waves beyond the hydrostatic regime. *Journal of Fluid Mechanics* **998**, A17.
- LAM, HENRI, DELACHE, ALEXANDRE & GODEFERD, FABIEN S 2020 Partitioning waves and eddies in stably stratified turbulence. *Atmosphere* **11** (4).
- LANCHON, NICOLAS & CORTET, PIERRE-PHILIPPE 2023 Energy spectra of nonlocal internal gravity wave turbulence. *Phys. Rev. Lett.* **131**, 264001.
- LANCHON, NICOLAS, MORA, DANIEL ODENS, MONSALVE, EDUARDO & CORTET, PIERRE-PHILIPPE 2023 Internal wave turbulence in a stratified fluid with and without eigenmodes of the experimental domain. *Physical Review Fluids* **8** (5), 054802.
- LAVAL, J.-P., MCWILLIAMS, J. C. & DUBRULLE, B. 2003 Forced stratified turbulence: Successive transitions with Reynolds number. *Phys. Rev. E* **68**, 036308.
- LE REUN, THOMAS, FAVIER, BENJAMIN, BARKER, ADRIAN J. & LE BARS, MICHAEL 2017 Inertial wave turbulence driven by elliptical instability. *Phys. Rev. Lett.* **119**, 034502.
- LE REUN, THOMAS, FAVIER, BENJAMIN & LE BARS, MICHAEL 2018 Parametric instability and wave turbulence driven by tidal excitation of internal waves. *Journal of Fluid Mechanics* **840**, 498–529.
- CLARK DI LEONI, P. & MININNI, P. D. 2015 Absorption of waves by large-scale winds in stratified turbulence. *Phys. Rev. E* **91**, 033015.
- L'VOV, V. S. & NAZARENKO, S. 2010 Discrete and mesoscopic regimes of finite-size wave turbulence. *Phys. Rev. E* **82**, 056322.
- LVOV, YURI & TABAK, ESTEBAN G 2004 A hamiltonian formulation for long internal waves. *Physica D: Nonlinear Phenomena* **195** (1), 106–122.
- LVOV, YURI V., POLZIN, KURT L., TABAK, ESTEBAN G. & YOKOYAMA, NAOTO 2010 Oceanic internal-wave field: Theory of scale-invariant spectra. *Journal of Physical Oceanography* **40** (12), 2605–2623.
- LVOV, YURI V., POLZIN, KURT L. & YOKOYAMA, NAOTO 2012 Resonant and near-resonant internal wave interactions. *Journal of Physical Oceanography* **42** (5), 669–691.
- LVOV, YURI V & TABAK, ESTEBAN G 2001 Hamiltonian formalism and the garrett-munk spectrum of internal waves in the ocean. *Physical review letters* **87** (16), 168501.
- MACKINNON, JENNIFER A., ZHAO, ZHONGXIANG, WHALEN, CAITLIN B., WATERHOUSE, AMY F., TROSSMAN, DAVID S., SUN, OLIVER M., LAURENT, LOUIS C. ST., SIMMONS, HARPER L., POLZIN, KURT, PINKEL, ROBERT, PICKERING, ANDREW, NORTON, NANCY J., NASH, JONATHAN D., MUSGRAVE, RUTH, MERCHANT, LYNNE M., MELET, ANGELIQUE V., MATER, BENJAMIN, LEGG, SONYA, LARGE, WILLIAM G., KUNZE, ERIC, KLYMAK, JODY M., JOCHUM, MARKUS, JAYNE, STEVEN R., HALLBERG, ROBERT W., GRIFFIES, STEPHEN M., DIGGS, STEVE, DANABASOGLU, GOKHAN, CHASSIGNET, ERIC P., BUIJSMAN, MAARTEN C., BRYAN, FRANK O., BRIEGLEB, BRUCE P., BARNA, ANDREW, ARBIC, BRIAN K., ANSONG, JOSEPH K. & ALFORD, MATTHEW H. 2017 Climate process team on internal wave-driven ocean mixing. *Bulletin of the American Meteorological Society* **98** (11), 2429–2454.

- McCOMAS, C HENRY & BRETHERTON, FRANCIS P 1977 Resonant interaction of oceanic internal waves. *Journal of Geophysical Research* **82** (9), 1397–1412.
- McLACHLAN, ROBERT I. & QUISP, G. REINOUT W. 2002 Splitting methods. *Acta Numerica* **11**, 341–434.
- MILES, JOHN W. 1961 On the stability of heterogeneous shear flows. *Journal of Fluid Mechanics* **10** (4), 496–508.
- MÜLLER, PETER, HOLLOWAY, GREG, HENY, FRANK & POMPHE, NEIL 1986 Nonlinear interactions among internal gravity waves. *Reviews of Geophysics* **24** (3), 493–536.
- NAZARENKO, S. 2011 *Wave Turbulence. Lecture Notes in Physics* 1. Springer Berlin Heidelberg.
- NEWELL, ALAN C & RUMPF, BENNO 2011 Wave turbulence. *Annual review of fluid mechanics* **43** (1), 59–78.
- OLBERS, DIRK J. 1976 Nonlinear energy transfer and the energy balance of the internal wave field in the deep ocean. *Journal of Fluid Mechanics* **74** (2), 375–399.
- PELINOVSKY, E. N. & RAEVSKY, M. A. 1977 Weak turbulence of the internal waves of the ocean. *Atm. Ocean Phys.-Izvestija* **13**, 187–193.
- PETROPOULOS, NICOLAOS, MASHAYEK, ALI & CAULFIELD, COLM-CILLE P. 2023 Turbulent disruption of density staircases in stratified shear flows. *Journal of Fluid Mechanics* **961**, A30.
- PHILLIPS, O.M. 1972 Turbulence in a strongly stratified fluid—is it unstable? *Deep Sea Research and Oceanographic Abstracts* **19** (1), 79–81.
- POLZIN, KURT L., NAVEIRA GARABATO, ALBERTO C., HUUSSEN, TYCHO N., SLOYAN, BERNADETTE M. & WATERMAN, STEPHANIE 2014 Finescale parameterizations of turbulent dissipation. *Journal of Geophysical Research: Oceans* **119** (2), 1383–1419, arXiv: <https://agupubs.onlinelibrary.wiley.com/doi/pdf/10.1002/2013JC008979>.
- REMMEL, MARK, SUKHATME, JAI & SMITH, LESLIE M. 2014 Nonlinear gravity-wave interactions in stratified turbulence. *Theoretical and Computational Fluid Dynamics* **28** (2), 131–145.
- RODDA, COSTANZA, SAVARO, CLÉMENT, DAVIS, GÉRALDINE, RENEUE, JASON, AUGIER, PIERRE, SOMMERIA, JOËL, VALRAN, THOMAS, VIBOUD, SAMUEL & MORDANT, NICOLAS 2022 Experimental observations of internal wave turbulence transition in a stratified fluid. *Phys. Rev. Fluids* **7**, 094802.
- ROGERS, T. M., LIN, D. N. C., McELWAIN, J. N. & LAU, H. H. B. 2013 Internal gravity waves in massive stars: Angular momentum transport. *The Astrophysical Journal* **772** (1), 21.
- SCOTT, J.F. & CAMBON, C. 2024 Evolution of weak, homogeneous turbulence with rotation and stratification. *Journal of Fluid Mechanics* **979**, A17.
- SHAVIT, MICHAL, BÜHLER, OLIVER & SHATAH, JALAL 2023 The role of sign indefinite invariants in shaping turbulent cascades. *arXiv preprint arXiv:2311.04183*.
- SHAVIT, MICHAL, BÜHLER, OLIVER & SHATAH, JALAL 2024 Turbulent spectrum of 2d internal gravity waves, arXiv: 2406.06010.
- SMITH, LESLIE 2001 Numerical study of two-dimensional stratified turbulence. *Contemp. Math.* **283**, 91.
- SMITH, LESLIE M. & WALEFFE, FABIAN 2002 Generation of slow large scales in forced rotating stratified turbulence. *Journal of Fluid Mechanics* **451**, 145–168.
- SMITH, STEFAN G LLEWELLYN & YOUNG, WR 2003 Tidal conversion at a very steep ridge. *Journal of Fluid Mechanics* **495**, 175–191.
- TAYLOR, J. R. & ZHOU, Q. 2017 A multi-parameter criterion for layer formation in a stratified shear flow using sorted buoyancy coordinates. *Journal of Fluid Mechanics* **823**, R5.
- VALLIS, GEOFFREY K 2017 *Atmospheric and oceanic fluid dynamics*. Cambridge University Press.
- WAITE, MICHAEL L. 2011 Stratified turbulence at the buoyancy scale. *Physics of Fluids* **23** (6), 066602.
- WHALEN, CAITLIN B, DE LAVERGNE, CASIMIR, NAVEIRA GARABATO, ALBERTO C, KLYMAK, JODY M, MACKINNON, JENNIFER A & SHEEN, KATY L 2020 Internal wave-driven mixing: Governing processes and consequences for climate. *Nature Reviews Earth & Environment* **1** (11), 606–621.
- YOKOYAMA, NAOTO & TAKAOKA, MASANORI 2019 Energy-based analysis and anisotropic spectral distribution of internal gravity waves in strongly stratified turbulence. *Phys. Rev. Fluids* **4**, 104602.
- ZAKHAROV, VLADIMIR E., L'VOV, VICTOR S. & FALKOVICH, GREGORY 1992 *Kolmogorov Spectra of Turbulence I. Springer Series in Nonlinear Dynamics* 1. Springer.
- ZHU, YING, SEMISALOV, BORIS, KRSTULOVIC, GIORGIO & NAZARENKO, SERGEY 2022 Testing wave turbulence theory for the Gross-Pitaevskii system. *Phys. Rev. E* **106** (1), 014205.